Journal of Power Sources 448 (2020) 227584

Contents lists available at ScienceDirect

Journal of Power Sources

journal homepage: www.elsevier.com/locate/jpowsour

High efficiency perovskite solar cells with tailorable surface wettability by surfactant

Tun Wang [a], Muyuan Xie [b], Sadeq Abbasi [a], Zhendong Cheng [a], Hong Liu [a,*], Wenzhong Shen [a,**]

[a] Key Laboratory of Artificial Structures and Quantum Control (Ministry of Education), Institute of Solar Energy, School of Physics and Astronomy, Shanghai Jiao Tong University, Shanghai, 200240, PR China
[b] Department of Chemistry, The Pennsylvania State University, University Park, PA, 16802, USA

HIGHLIGHTS

- High PCE of 20.15% is achieved from SDBS-treated perovskite solar cells.
- Surface wettability of NiO_x films can be regulated by adjusting SDBS concentration.
- SDBS boosts perovskite crystallization and reduces interfacial defects.

ARTICLE INFO

Keywords:
Perovskite solar cells
Interface modification
High open-circuit voltage
Hysteresis-free

ABSTRACT

Perovskite solar cells based on nickel oxide (NiO_x) attract tremendous attention and develop rapidly. Nevertheless, they are plagued by charge recombination and extraction loss at interfaces between the perovskite absorber and the charge transport layers. Herein, an ultrathin sodium dodecyl benzene sulfonate (SDBS) film is introduced between the perovskite absorber and the NiO_x hole transport layer (HTL) to reduce interfacial and extraction losses. The modification on the NiO_x HTL by SDBS surfactant can effectively tailor the quality of the perovskite film with larger grain size and better crystallinity by regulating the wettability of the NiO_x surface with varied concentration of SDBS solution. Moreover, the charge separation and extraction in the perovskite/HTL interface are enhanced after SDBS treatment on NiO_x HTL characterized by electrochemical impedance characterization. As a consequence, these benefits contribute to high power conversion efficiency (PCE) of 20.15%, in comparison with PCE of 16.26% for the reference device. It is hoped that this work will provide new perspectives for preparing perovskite solar cells with an unprecedented performance and the opportunity for commercialization.

1. Introduction

Hybrid organic-inorganic perovskite materials have attracted extensive attention in recent years due to a series of advantages, such as high light absorption coefficient [1], large carrier mobility and diffusion length [2,3], and adjustable bandgap [4], making it possible to commercially applied in photovoltaic field as a leading contender. Even though the power conversion efficiency (PCE) of champion perovskite solar cells (PSCs) has reached over 25% according to the latest reports [5,6], the short-circuit photocurrent density (J_{SC}) and open-circuit voltage (V_{OC}) are still far smaller than that of the theoretical limits (26 mA cm^{-2} and 1.3 V, respectively) [7,8]. In view of this, various methods have been proposed to improve the light harvesting and film quality of perovskite layer, such as increasing crystallinity, reducing pinhole defects, and improving the contact interfaces between perovskite layer and other functional layers [9–11]. According to the previous publications, the photovoltaic parameters of solar cells are extremely related to the recombination of defects in the bulk or on the surface of the perovskite layer [12]. Benefiting from the enlarging grains and improving crystallinity of the perovskite films with recent rapid progress in morphology regulation, the carrier diffusion length can be much longer than the light penetration length in single crystals or even in polycrystalline perovskite thin films prepared by solution-derived process, which leads to negligible charge recombination in the grain

* Corresponding author.
** Corresponding author.
E-mail addresses: liuhong@sjtu.edu.cn (H. Liu), wzshen@sjtu.edu.cn (W. Shen).

https://doi.org/10.1016/j.jpowsour.2019.227584
Received 26 September 2019; Received in revised form 5 November 2019; Accepted 7 December 2019
Available online 10 December 2019

interior [13]. Therefore, suppression of defects and minimizing charge recombination at the interfaces are critical for further enhancing the performance of PSCs towards their photovoltaic limits.

Typically, interfacial passivation is one of the most important and effective approaches to inhibit charge recombination in defects, yielding both improved V_{OC} and device stability [14]. For example, appropriate chlorine atoms on the surface of perovskite layer can suppress charge recombination by strong binding at the perovskite/charge transport layer interface [15]. Besides, excess PbI_2 in the perovskite layer, on the surface or between grain boundaries can effectively reducing the possibility of recombination by forming appropriate matching energy levels and suppressing non-radiative losses [16,17]. Recently, insulating polymers such as polystyrene (PS), poly(methyl methacrylate) (PMMA) and Teflon have been extensively researched as tunneling passivation layer either before or after the perovskite film deposition [13,18]. The inserted passivation layer has contributed to improved crystallinity and morphology of perovskite film, filling of pinholes and grain boundaries, and unspecified passivation of surface traps [19,20]. Similarly, Jen et al. used a series of benzoic acid assembled monolayers to passivate the surface defects [21]. However, these materials need to be dissolved in toxic organic solvents such as chlorobenzene or dimethyl formamide to prepare the precursor solution and then spin-coated on substrate in a glovebox filled with nitrogen, which is environmentally harmful and costly. Even though a greener way of modification via 5-AVA aqueous solution for improving efficiency of PSCs has been proposed by Chen et al. [22], the time-consuming treatment (~12 h) is not a good option for real application.

Herein, to address these drawbacks, we propose to passivate perovskite film by inserting ultrathin sodium dodecyl benzene sulfonate (SDBS) film between perovskite and hole transport layer (HTL). As an anionic surfactant, SDBS solution (dissolved in deionized water) can regulate the surface wettability of electrochemically deposited NiO_x HTL as well as the morphology of the grown perovskite layer in the following process. The ultrathin passivation layer dramatically restrains interface recombination, as evidenced by enhanced V_{OC} and J_{SC}, and corroborated by photoluminescence (PL) imaging (steady and time-resolved), electrochemical impedance spectroscopy, and dark current measurements. SDBS-passivated PSCs have been fabricated with a champion efficiency of 20.15% and infusive V_{OC} of 1.124 V without hysteresis. We also find that the carrier recombination and efficiency loss are significantly dominated by the concentration of SDBS solution spin-coated on the NiO_x HTL. Consequently, this work not only demonstrates a green, convenient and effective interface passivation approach to improve the performance of PSCs, but also provides new physical insights that surfactant could play a unique promoting role in device performance.

2. Experimental section

2.1. Device fabrication

The etched fluorine-doped SnO_2 (FTO) glass substrates were sequentially cleaned by acetone, isopropanol (IPA), ethanol and deionized water with the assistance of ultrasonication for 15 min, respectively. After being dried by nitrogen flow, the substrates were treated by ultraviolet/ozone for 20 min to remove the organic residues. The nickel oxide film as a hole transport layer was deposited on the FTO substrate by electrochemical deposition method and then annealed at 300 °C for 2 h, which can be found in our previous work [23]. After that, sodium dodecyl benzene sulfonate (SDBS) solution (dissolved in deionized water) was spin-coated on the NiO_x film and then the samples were heated at 80 °C for 10 min to remove the residual moisture. Subsequently, the samples were moved to the glovebox filled with high purity nitrogen to prepare perovskite layer. The perovskite film was prepared by the one-step method. The details can be seen in our previous publications [23,24]. Briefly, the perovskite precursor solution composed of 1 M PbI_2 and CH_3NH_3I (1:1/n:n) in γ-butyrolactone (GBL) and dimethyl sulfoxide (DMSO) (7:3/v:v) was spin-coated on the NiO_x layer consecutively at 500 and 4000 rpm for 12 and 30 s, respectively. 150 μL chlorobenzene (CB) was rapidly dripped onto the perovskite precursor 10 s before the end of the spin-coating process and then the samples were put into an airtight glass pot and annealed at 100 °C for 10 min. Thereafter, the phenyl-C61-butyric acid methyl ester (PCBM) solution (20 mg mL^{-1} dissolved in CB) and bathocuproine (BCP) solution (0.5 mg mL^{-1} in IPA) were then sequentially spin-coated onto the perovskite layer at 2000 rpm for 30 s and 4000 rpm for 30 s, respectively. Finally, silver electrodes with thickness of ~120 nm were formed by thermal evaporation under high vacuum (lower than 1×10^{-4} Pa). The active area of the PSC device is 5 mm*5 mm.

2.2. Characterization and measurement

The contact angle of the SDBS-treated NiO_x film was measured by a contact angle analyzer (DSA100, KRUSS, Germany). The surface morphology of the samples has been characterized by scanning electron microscope (SEM, Carl Zeiss, Germany) and atomic force microscope (AFM, Nanoscope IIIa Multimode, USA). The crystallinity of the perovskite films has been characterized by X-ray diffraction (XRD, D8 ADVANCE, Germany). The steady-state photoluminescence (PL) and time-resolved photoluminescence (TRPL) spectra of the samples have been tested by Steady-State & Time-Resolved Fluorescence Spectrofluorometer (QM/TM/IM, PTI, USA) with an excitation laser of 460 nm. The electrochemical impedance spectroscopy (EIS) has been carried out at potentials of 0.8 V in the dark with frequencies sweeping from 1 MHz to 10 Hz by an electrochemical workstation (CS350H, Corrtest, China) and the oscillation potential amplitude was 10 mV. The photocurrent density-voltage (*J-V*) curves of the prepared solar cells have been measured under standard 1 sun AM 1.5G with a solar simulator (Newport, 2612A) calibrated with a Newport 91150 V reference silicon cell system in ambient air (at ~22 °C and relative humidity of ~60%). $J-V$ curves were recorded by means of reverse (from 1.2 to −0.2 V) or forward (from −0.2 to 1.2 V) scanning with scan rate of 0.1 V s^{-1}. The external quantum efficiency (EQE) spectra of PSCs have been measured using a quantum efficiency measurement system (QEX10, PV measurements, USA).

3. Results and discussion

The mesoporous NiO_x film was firstly deposited on the cleaned FTO substrate through electrochemical deposition process, the detailed information can be found in our previous works [23,24]. Then SDBS solution with different concentrations (C_{SDBS} = 0.05, 0.20, 1 and 10 mg mL^{-1}) were spin-coated on the NiO_x film in ambient air. The presence of the SDBS film was almost imperceptible on the NiO_x film according to the scanning electron microscope (SEM) images (Fig. S1 in supporting information), but the surface wettability of the NiO_x film was significantly regulated by the concentration of SDBS solution (Fig. 1a–e). The contact angle of the pristine NiO_x film is 41.1°, while that of the NiO_x/SDBS sample is as high as 127.1° at C_{SDBS} = 0.2 mg mL^{-1} and it rapidly decreases with the increasing concentration of SDBS solution. The increasing contact angle versus SDBS concentration in low concentration range (<0.2 mg mL^{-1}) should be ascribed to the interaction between polar benzenesulfonyl groups in SDBS anions and NiO_x mesoporous film via electrostatic force, leaving the hydrophobic long dodecyl groups pointing away from the substrate (Fig. S2 in supporting information) [25]. But this situation could be reversed that the hydrophobic groups will turn to face the NiO_x surface through a hydrophobic interaction at even higher SDBS concentration [26], leaving the polar groups exposed outside and therefore reducing the contact angle. The perovskite absorber was then grown on the SDBS-treated NiO_x film by one-step method in a glovebox. Fig. 1f–j show the top-view SEM images of $CH_3NH_3PbI_3$ ($MAPbI_3$) films deposited on NiO_x treated by SDBS solution with different concentrations (0.05, 0.2, 1 and 10 mg mL^{-1}). It is

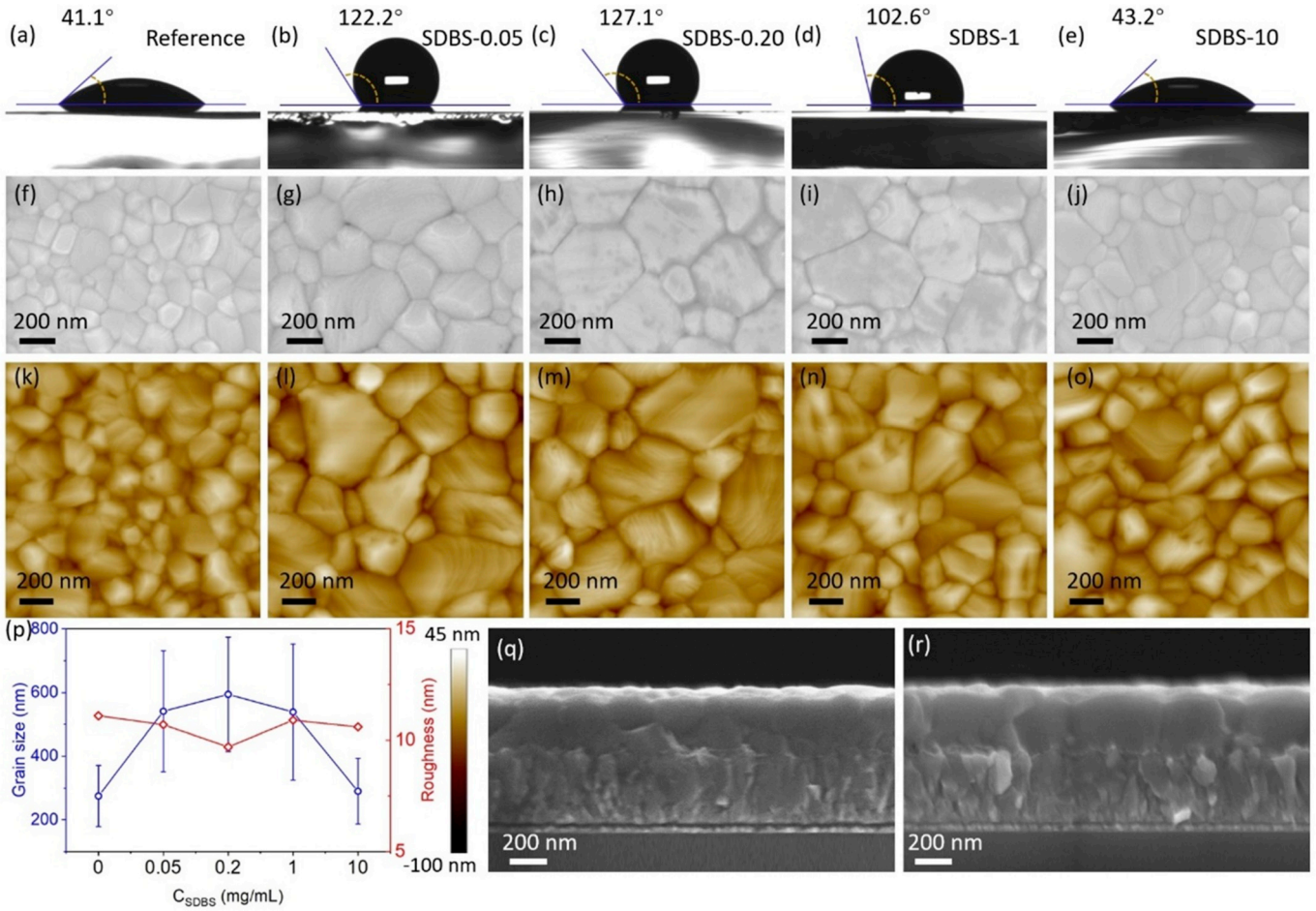

Fig. 1. The contact angle of water on the NiO_x/SDBS film with different concentrations (mg mL^{-1}) of SDBS: (a) 0, (b) 0.05, (c) 0.20, (d) 1 and (e) 10. Top view SEM and AFM images of perovskite films deposited on NiO_x/SDBS film with different concentrations (mg mL^{-1}) of SDBS: 0 (f and k), 0.05 (g and l), 0.20 (h and m), 1 (i and n) and 10 (j and o). (p) Statistics of grain size and surface roughness of perovskite films deposited on NiO_x/SDBS film with different concentrations of SDBS solution. Cross-sectional SEM images of perovskite layers grown on NiO_x film (q) without and (r) with SDBS layer.

clear that the perovskite grain size can be significantly affected by the concentration of SDBS solution. The average grain size of the reference perovskite film deposited on the pristine NiO_x film is only about 290 nm, it is dramatically increased to as large as 600 nm when the concentration of the SDBS solution is 0.2 mg mL^{-1}. However, further increasing the SDBS concentration leads to smaller perovskite grain size. This may be caused by the abnormally improved surface wettability of the NiO_x film. According to previous literatures [27], the enhanced non-wetting property can significantly reduce the surface tension dragging force applying on the perovskite film, thus resulting in higher grain boundary mobility and larger grain size. The perovskite films with large grain size and invisible pinholes are crucial for suppressing charge recombination at interface and grain boundaries, which can guarantee the effective extraction and transport for photoinduced carriers form the perovskite absorber to the corresponding charge transport layer [28].

Moreover, the atomic force microscope (AFM) was also utilized to observe the surface morphologies of the perovskite films (Fig. 1k-o). Fig. 1p summarizes the statistics of the grain size and surface roughness of the representative perovskite films grown under different conditions. The root-mean-square (RMS) values of roughness were slightly affected by the varying concentration of SDBS solution and the perovskite film deposited on the NiO_x/SDBS-0.2 film exhibits the smallest roughness of 9.7 nm. The smoother surface will induce less defects and trap states at the perovskite/electron transport layer interface and thus cause less trap-assisted carrier recombination [29]. As illustrated in the cross-sectional SEM images in Fig. 1q–r, the uniform perovskite films with closely packed grain boundaries are stacked on the pristine NiO_x (Fig. 1q) and SDBS-treated NiO_x film (Fig. 1r). Unlike the reference perovskite film, the perovskite film grown on the SDBS-treated NiO_x HTL is consisted of a monolithic $MAPbI_3$ layer, leading to lower density of grain boundaries and defects [30].

The light-harvesting capacity of the perovskite film has been considered to be related to the J_{SC} of the devices [31], therefore, ultraviolet–visible (UV–Vis) absorption spectra were characterized to evaluate the optical absorption property of the perovskite films grown on the NiO_x film treated by SDBS surfactant. As can be seen from Fig. 2a, all the samples exhibit similar absorption curves in shape. The inset shows the enlarged absorption spectra at the wavelength range from 450 nm to 480 nm, indicating that the absorption of perovskite grown on SDBS-treated NiO_x film has been enhanced compared to the reference sample that directly deposited on NiO_x film, though not significantly. It's worth noting that the sample with 0.2 mg mL^{-1} of SDBS represents the most obvious absorption enhancement, this could be attributed to the significantly increased perovskite grain size [32].

Furthermore, the crystallization of perovskite films has been confirmed by X-ray diffraction (XRD) analysis and the characteristic patterns of the perovskite films with different concentrations of SDBS are shown in Fig. 2b. The three distinct peaks at 14.2°, 28.5° and 31.9° indicated by stars can be assigned to (110), (220) and (310) lattices planes of $MAPbI_3$, respectively [33]. The intensity ratio between perovskite and FTO (14.2° and 37.8°, respectively) has been significantly strengthened from 4.13 to 5.37 after SDBS-0.2 treatment on NiO_x

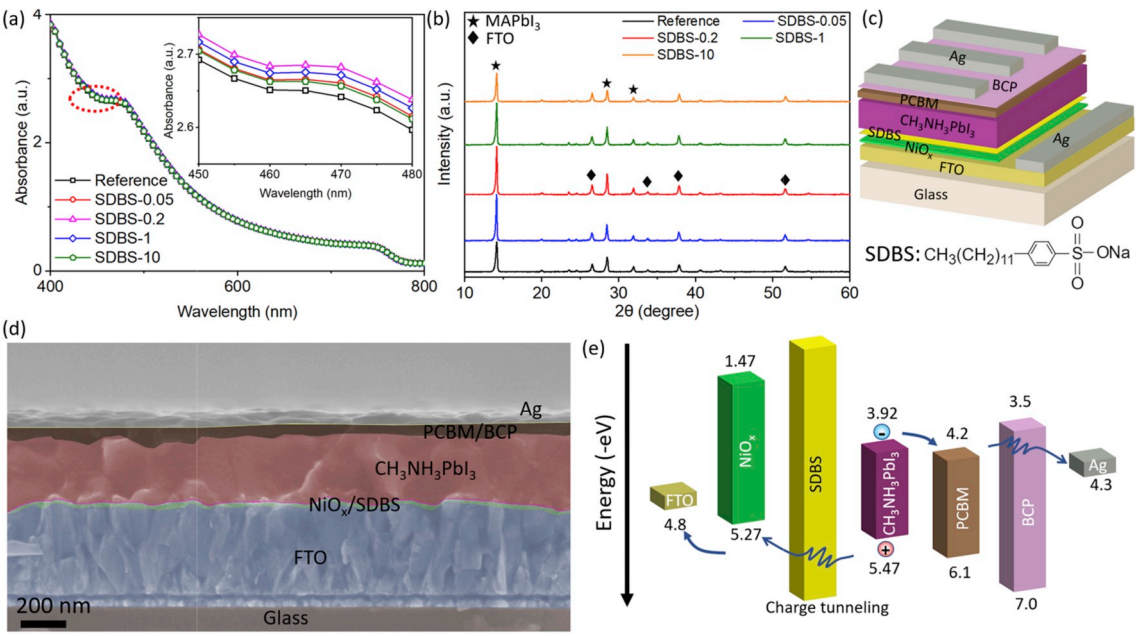

Fig. 2. (a) Optical absorbance and (b) XRD patterns of the perovskite films deposited on NiO_x film treated by different concentrations of SDBS solution. (c) Three-dimensional schematic architecture of the inverted PSC device and the chemical structure of SDBS. (d) False color cross-sectional SEM image and (e) schematic representation of the energy band diagram of a typical solar cell. (For interpretation of the references to color in this figure legend, the reader is referred to the Web version of this article.)

film, together with the decreasing full width at half maximum (FWHM) of perovskite (110) peak from 0.27° to 0.19° (details can be seen in Fig. S3b), which demonstrates better crystallinity of the perovskite film grown on the SDBS-treated NiO_x. Then we successively deposited PCBM, BCP and silver layers on the perovskite film as electron transport layer (ETL), hole blocking layer and top electrodes, respectively. The fabricated PSCs exhibit an inverted heterojunction structure of FTO/-NiO_x/SDBS/$CH_3NH_3PbI_3$/PCBM/BCP/Ag (Fig. 2c). The cross-sectional SEM image of a typical PSC device shown in Fig. 2d reveals that the perovskite layer is compactly composed of one grain and no pinholes exist at the interfaces between perovskite and charge transport layer, which effectively restricts charge recombination by preventing direct contact between the HTL and ETL, thus leading to lower shunt-current leakage in devices. The energy band diagram of our device is depicted in Fig. 2e. The ultrathin SDBS film could suppress electronic transmission channel and ensure effective hole transport because of charge tunneling effect [29].

Considering the influenced crystallization of perovskite grown on SDBS-treated NiO_x film, the thickness of the SDBS film could affect the hole-extraction property and thus the PCE. Fig. 3a shows the

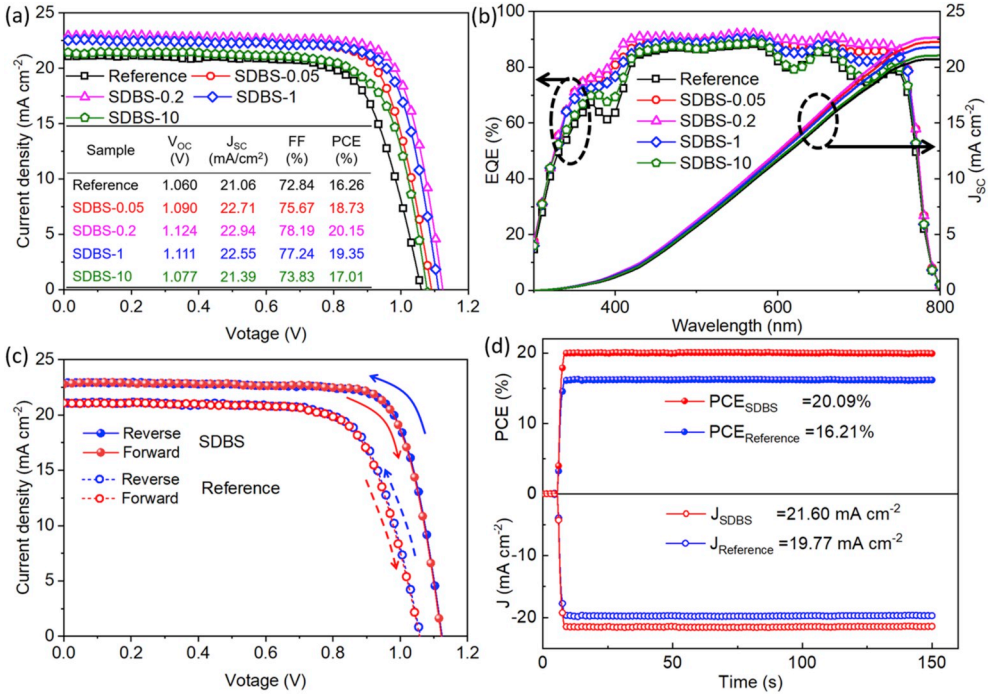

Fig. 3. (a) *J-V* curves and (b) EQE spectra and the corresponding integrated current densities of PSCs with SDBS treatment at different concentrations. (c) *J-V* curves of the champion PSCs based on pristine and SDBS-treated NiO_x. The blue and red curves represent the reverse and forward scanning directions, respectively. (d) Stable current density and PCE of the PSCs based on pristine and SDBS-treated NiO_x measured when the devices were applied bias potential at 0.82 and 0.93 V, respectively. (For interpretation of the references to color in this figure legend, the reader is referred to the Web version of this article.)

photocurrent density-voltage (*J-V*) curves of PSCs by inserting a thin SDBS layer with different thicknesses, which can be well regulated by varying the concentration of SDBS solution in the spin-coating process. The corresponding photovoltaic parameters are listed in the inset. It is observed that the reference device without SDBS treatment on NiO_x film has a quite ordinary PCE of 16.26% (with a V_{OC} of 1.060 V, a J_{SC} of 21.06 mA cm^{-2} and a fill factor (FF) of 72.84%), which represent a typical performance of NiO_x-based perovskite devices [34,35]. In a striking contrast, the devices with SDBS layer exhibit significantly enhanced photovoltaic parameters. With the concentration of the SDBS precursor solution varying from 0.05 to 0.2, 1 and 10 mg mL^{-1}, the devices showed higher V_{OC} of 1.090, 1.124, 1.111, 1.077 V and higher J_{SC} of 22.71, 22.94, 22.55, 21.39 mA cm^{-2}, respectively. At the meantime, the corresponding FF values of the devices were increased to 75.67%, 78.19%, 77.24% and 73.83%, respectively. As a result, the champion device with SDBS-0.2 exhibits the highest PCE of 20.15%. Fig. 3b presents the external quantum efficiency (EQE) spectra of the corresponding solar cells. The EQE values of the SDBS-treated devices are much higher than that of the reference sample in the wavelengths from 350 to 450 nm and 600–750 nm. This could be attributed to the enhanced optical absorption of perovskite and reduced charge recombination at the HTL/perovskite interface because of enlarged perovskite crystal size and improved crystallization [36,37]. The integrated J_{SC} values from the EQE spectra are 20.73, 22.26, 22.65, 21.80 and 21.05 mA cm^{-2} for SDBS-treated NiO_x film with the concentration of 0, 0.05, 0.2, 1 and 10 mg mL^{-1}, respectively, which are highly agreement with the measured J_{SC}.

We also examined the hysteresis effect of our devices under forward and reverse scanning conditions. As shown in Fig. 3c, the overlapping *J-V* curves indicate negligible hysteresis for the both champion devices with or without SDBS treatment. Moreover, the corresponding photovoltaic parameters listed in Table 1 shows that the hysteresis of the SDBS-incorporated PSCs is slightly smaller than that of the reference PSCs. This may be attributed to the reduced overall bulk defect density and suppressed charge trapping after introducing the SDBS layer which can effectively enlarge the perovskite crystal size and improve the crystallization as shown in Figs. 1 and 2 [38]. As shown in Fig. 3d, the steady-state current density and PCE of the champion devices were recorded using maximum power point (MPP) tracking under simulated AM 1.5G sunlight of 100 mW cm^{-2}. The devices exhibit stable PCE outputs of 20.09% and 16.21% for the SDBS-treated and reference PSCs measured at bias potential 0.93 and 0.82 V, respectively.

To evaluate the reproducibility of our devices, we then fabricated and measured 25 devices in each case and their statistical performance is summarized in Fig. 4. The reference devices have an average V_{OC} of 1.056 V, a J_{SC} of 20.85 mA cm^{-2}, an FF of 71.50%, and a PCE of 15.73%. It is clear that the PSCs with SDBS film show higher average PCE than that of the reference samples, with the improvement from V_{OC}, J_{SC} and FF. The enhancement of V_{OC} and J_{SC} should be related to the effective charge transfer and the trap-state passivation by SDBS ultrathin film. High FF value (>75%) usually means the absence of large carrier extraction/injection barrier at the interface between the perovskite and HTL/ETL [39]. The best-performing cells modified with SDBS-0.2 achieve the highest average PCE of 19.41%, with remarkably enhanced average V_{OC} of 1.118 V, J_{SC} of 22.65 mA cm^{-2} and FF of 76.69%.

To understand the charge transfer efficiency from the perovskite absorber to the HTL, steady-state photoluminescence (PL) and time-resolved PL (TRPL) spectra were successively characterized. As shown in Fig. 5a, the PL intensity of perovskite deposited on the NiO_x/SDBS film is remarkably quenched compared to that of the reference sample (the perovskite was directly grown on the NiO_x film). The strong PL quenching demonstrates the efficient charge transfer form perovskite absorber to NiO_x HTL [40]. Fig. 5b shows the normalized TRPL for perovskite films deposited on the NiO_x HTL with or without SDBS treatment. The TRPL spectra have been typically used to evaluate the charge recombination at the perovskite/HTL interface and they can be fitted with a biexponential decay function $I = A_1\exp(-(t-t_0)/\tau_1) + A_1\exp(-(t-t_0)/\tau_2) + I_0$, where τ_1 and τ_2 represent the first and second order decay times, A_1 and A_2 are the weighting coefficients of each decay channel [41]. The fitted parameters are summarized in Table S1. Generally, the non-radiative fast-decay lifetime (τ_1) and radiative slow-decay lifetime (τ_2) are attributed to the quenching and the radiative recombination of free charge carriers at the HTL/perovskite interface, respectively [42]. The pristine perovskite film has an average lifetime (τ_a) of 11.4 ns. After introducing the SDBS film between perovskite and NiO_x HTL, the average decay time was decreased to 5.5 ns, suggesting that photoinduced carriers are more efficiently extracted from the perovskite absorber to NiO_x HTL [43].

The charge carrier transport and recombination properties of our solar cells were further examined using electrochemical impedance spectroscopy (EIS). Fig. 5c shows the Nyquist plots of the devices with or without SDBS layer in the frequency sweeping from 1 MHz to 10 Hz. The EIS plots can be well fitted using an equivalent circuit shown in the inset. The circuit includes a series resistance (R_s), and a contact resistance (R_{co}) and a recombination resistance (R_{rec}). Typically, the right end of the semicircle relates the recombination resistance in the device [44]. The SDBS-based deice shows a higher recombination resistance (2093 Ω) as compared to that of the reference device (297 Ω), indicating a lower recombination rate in the SDBS-treated solar cells. These observations reveal SDBS surfactant indeed exhibiting positive passivation effect on the HTL/perovskite interface, which will be expected to yield higher short current density and fill factor [45].

To further understand the effect of the SDBS treatment on the NiO_x HTL, the capacitance-voltage (C–V) characteristics were obtained from Mott-Schottky measurement. As shown in Fig. 5d, the built-in potential (V_{bi}) can be derived from the x-intercept of the fitting line in the Mott-Schottky plot. The V_{bi} of the SDBS-based device is 0.1 V higher than that of the reference sample, which will be beneficial for accelerating charge dissociation and avoid charge accumulation at HTL/perovskite interface, thereby attributing to higher V_{OC} [46].

Moreover, the hole-only perovskite devices with FTO/NiO_x(/SDBS)/perovskite/Ag were fabricate to evaluate the charge trap state density at the HTL/perovskite interface by space-charge-limited current (SCLC) method. The *J-V* curves of the devices were measured under dark condition and the results are shown in Fig. 6a. The defect density (n_{trap}) can be calculated from the equation $n_{trap} = 2\varepsilon\varepsilon_0 V_{TFL}/(eL^2)$, where ε is the relative dielectric constant of $CH_3NH_3PbI_3$ and ε_0 is the vacuum permittivity, V_{TFL} represents the trap-filled limit voltage and can be derived from the intersection of the two fitting lines in ohmic and trap-filled limit regions, e and L are the electronic charge and the thickness of the perovskite layer [29]. The perovskite film deposited on NiO_x/SDBS exhibits a defect density of ~4.29×10^{15} cm^{-3}, which is lower than that of the reference perovskite film directly grown on the NiO_x HTL (~5.23×10^{15} cm^{-3}). The reduced defect density is mainly due to the enlarged grains and the decreased boundaries and is well consistent with our *J-V* measurement results [47]. The lower defect density is beneficial to increase the mean carrier diffusion length [48], which could ensure the charge transportation through the perovskite layer without too much obstacles and it also confirms that SDBS passivation is an effective procedure to improve the photovoltaic performance of PSCs.

Finally, we compared long-term stability of the PSCs based on SDBS and reference devices. The unencapsulated solar cells were stored in a drying cabinet with the relatively humidity of ~2% and temperature of

Table 1
Photovoltaic parameters of the PSCs with or without SDBS treatment.

Sample	Scan direction	V_{OC} (V)	J_{SC} (mA cm^{-2})	FF (%)	PCE (%)
Reference	Reverse	1.060	21.06	72.84	16.26
	Forward	1.057	21.06	72.44	16.13
SDBS	Reverse	1.124	22.94	78.19	20.15
	Forward	1.122	22.90	78.41	20.14

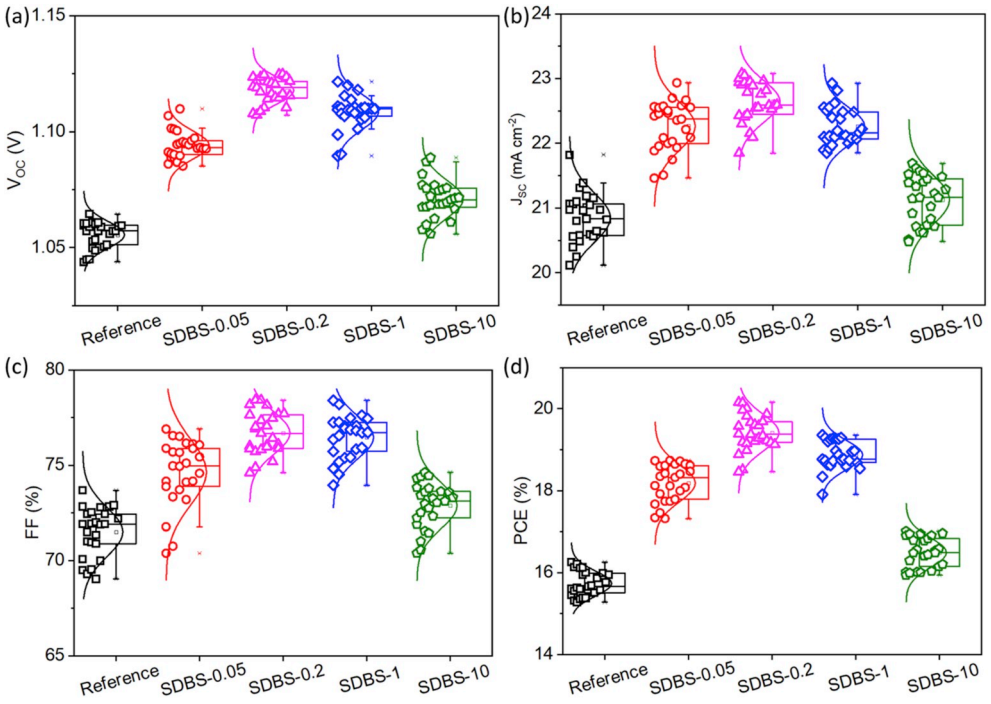

Fig. 4. Statistical distribution of the photovoltaic parameters for reference and SDBS-treated solar cells: (a) V_{OC}, (b) J_{SC}, (c) FF, and (d) PCE.

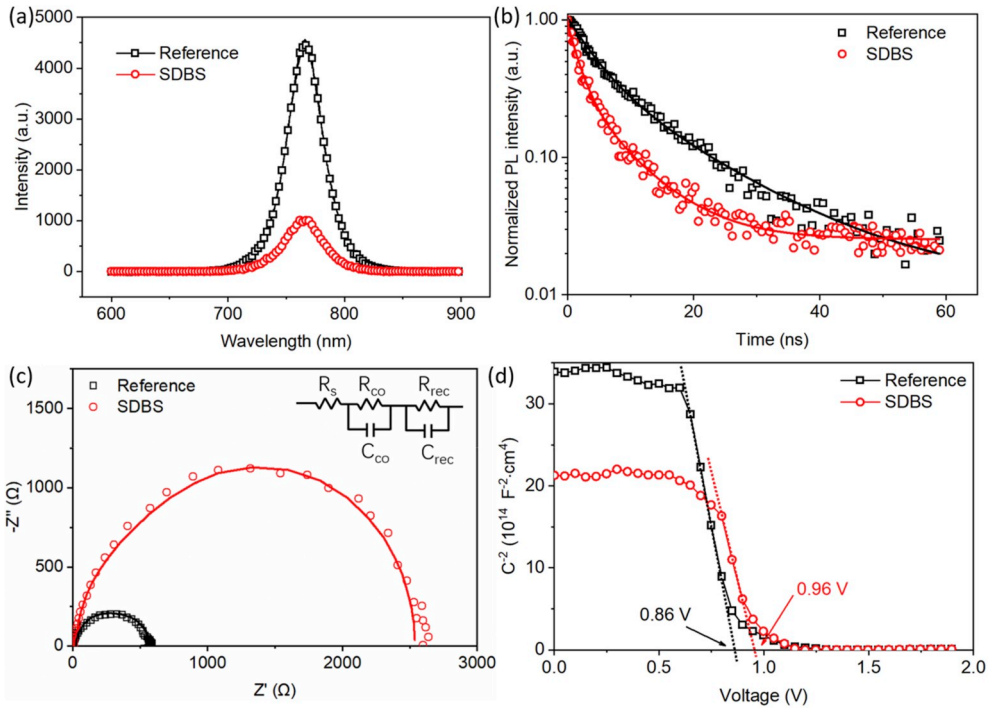

Fig. 5. (a) Steady photoluminescence (PL) and (b) time-resolved PL spectra of the perovskite films deposited on NiO_x film treated by different concentrations of SDBS solution. (c) Nyquist plots for the PSCs measured with a bias of 0.8 V under dark condition. (d) The Mott-Schottky curves of the devices with the frequency of 1 MHz under dark condition.

22 °C. The performance of the cells after different storage times is shown in Fig. 6b. Both devices exhibit similar stability patterns without obvious degradation in the first 3 weeks. After that, the PCE values slowly decrease, which is correlated to the degradation of the perovskite film [49]. The SDBS-based devices remained 96% of its initial value after 42 days storage, while the reference PSCs degraded to 92%. The output efficiency of the solar cells by tracking the maximum power point under AM 1.5 simulated light also shows similar stability after 42 days storage (Fig. S4). Compared to our previous work on the UV-ozone treated NiO_x solar cells with 84% of its original efficiency after 40 days storage [24], the SDBS-based solar cells exhibit much higher stability, which can be attributed to the improved perovskite film quality with larger grain size and less defects because of the passivation effect, which reduces the probability of water penetration and degradation of perovskite layer

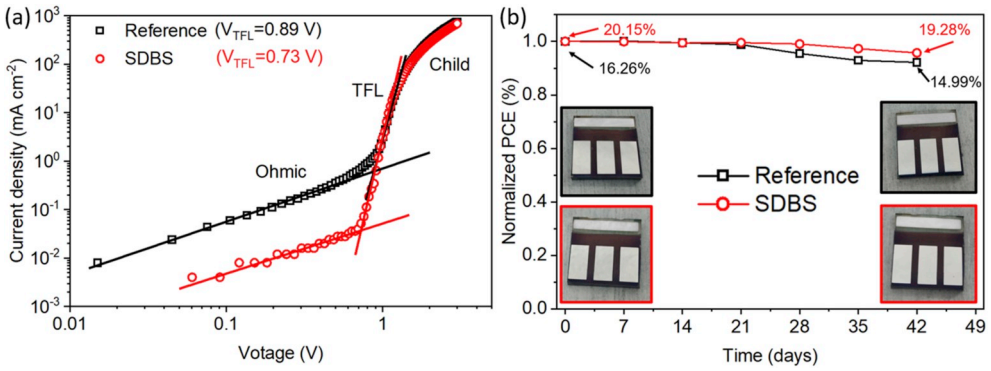

Fig. 6. (a) The representative dark J-V plots of the hole-only perovskite devices. Three regions can be distinguished according to different slope values: Ohmic (n = 1), Child region (n = 2) and trap-filled limited (TFL) region (n > 2). (b) The stability measurement of bare PSCs without any encapsulation stored in a drying cabinet of ~2% humidity in the dark. The insets are the real device images at the start and end of the long-term storage.

[30]. Our devices show comparable long-term stability with other reported NiO_x-based PSCs without encapsulation [50,51], the details are listed in Table S2.

Besides, the UV-ozone treatment on NiO_x film can only change the surface wettability from hydrophobic to hydrophilic, while this work shows a invertible strategy for controlling surface wettability from hydrophilic to hydrophobic and vice versa by simply controlling the concentration, which exhibits broader potential applications not just in solar cell fabrication, such as self-cleaning coating, flexible printed electronics, surface catalysis, etc. [52–54].

4. Conclusions

In summary, we have developed a strategy to improve the photovoltaic efficiency and stability of PSCs by introducing SDBS surfactant between perovskite absorber and NiO_x HTL. The SDBS surfactant could adjust the surface wettability of NiO_x HTL, which results in fully covered perovskite films with improved crystallization and enhanced grain size through a single-step spin coating method. Furthermore, the ultrathin SDBS film can significantly suppress the charge recombination, and efficiently extract the holes to the NiO_x HTL. A champion PSC achieves PCE up to 20.15% with a high V_{OC} of 1.124 V, which is 24% higher than that of the pristine device (16.26%). These results indicate that SDBS surfactant is beneficial to suppress recombination loss at perovskite surfaces.

Declaration of competing interest

The authors declare that they have no known competing financial interests or personal relationships that could have appeared to influence the work reported in this paper.

Acknowledgement

This work was supported by the National Natural Science Foundation of China (11834011, 11674225, 11474201, and 11204176).

Appendix A. Supplementary data

Supplementary data to this article can be found online at https://doi.org/10.1016/j.jpowsour.2019.227584.

References

[1] Q. Wang, N. Phung, D. Di Girolamo, P. Vivo, A. Abate, Energy Environ. Sci. 12 (2019) 865–886.
[2] S. Dong, A. Valerio, C. Riccardo, Y. Mingjian, A. Erkki, B. Andrei, C. Yin, H. Sjoerd, R. Alexander, K. Khabiboulakh, Science 347 (2015) 519–522.
[3] Q. Dong, Y. Fang, Y. Shao, P. Mulligan, J. Qiu, L. Cao, J. Huang, Science 347 (2015) 967–970.
[4] A. Sadhanala, S. Ahmad, B. Zhao, N. Giesbrecht, P.M. Pearce, F. Deschler, R. L. Hoye, K.C. Godel, T. Bein, P. Docampo, S.E. Dutton, M.F. De Volder, R.H. Friend, Nano Lett. 15 (2015) 6095–6101.
[5] M. Kim, G.-H. Kim, T.K. Lee, I.W. Choi, H.W. Choi, Y. Jo, Y.J. Yoon, J.W. Kim, J. Lee, D. Huh, Joule 3 (2019) 1–14.
[6] NREL, Efficiency chart (accessed August 2019), https://www.nrel.gov/pv/assets/pdfs/best-research-cell-efficiencies.20190802.pdf.
[7] N. Ahn, D.Y. Son, I.H. Jang, S.M. Kang, M. Choi, N.G. Park, J. Am. Chem. Soc. 137 (2015) 8696–8699.
[8] W.E.I. Sha, X. Ren, L. Chen, W.C.H. Choy, Appl. Phys. Lett. 106 (2015) 221104.
[9] Y. Wang, P. Wang, X. Zhou, C. Li, H. Li, X. Hu, F. Li, X. Liu, M. Li, Y. Song, Adv. Energy Mater. 8 (2018) 1702960.
[10] R. Cheng, C.C. Chung, H. Zhang, Z. Zhou, P. Zhai, Y.T. Huang, H. Lee, S.P. Feng, Small 15 (2019) 1804465.
[11] T. Singh, T. Miyasaka, Adv. Energy Mater. 8 (2018) 1700677.
[12] Q. Jiang, Y. Zhao, X. Zhang, X. Yang, Y. Chen, Z. Chu, Q. Ye, X. Li, Z. Yin, J. You, Nat. Photonics 13 (2019) 460–466.
[13] Q. Wang, Q. Dong, T. Li, A. Gruverman, J. Huang, Adv. Mater. 28 (2016) 6734–6739.
[14] P. Zhao, B.J. Kim, H.S. Jung, Mater. Today Energy 7 (2018) 267–286.
[15] H. Tan, A. Jain, O. Voznyy, X. Lan, G.D.A. Fp, J.Z. Fan, R. Quintero-Bermudez, M. Yuan, B. Zhang, Y. Zhao, Science 355 (2017) 722–726.
[16] Y. Zhao, Q. Li, W. Zhou, Y. Hou, Y. Zhao, R. Fu, D. Yu, X. Liu, Q. Zhao, Sol. RRL 3 (2019) 1800296.
[17] Q. Chen, H. Zhou, T.B. Song, S. Luo, Z. Hong, H.S. Duan, L. Dou, Y. Liu, Y. Yang, Nano Lett. 14 (2014) 4158–4163.
[18] D. Bi, C. Yi, J. Luo, J.D. Décoppet, F. Zhang, S.M. Zakeeruddin, X. Li, A. Hagfeldt, M. Grätzel, Nat. Energy 1 (2016) 16142.
[19] J. Peng, J.I. Khan, W. Liu, E. Ugur, T. Duong, Y. Wu, H. Shen, K. Wang, H. Dang, E. Aydin, X. Yang, Y. Wan, K.J. Weber, K.R. Catchpole, F. Laquai, S. De Wolf, T. P. White, Adv. Energy Mater. 8 (2018) 1801208.
[20] T. Wang, Z. Cheng, Y. Zhou, H. Liu, W. Shen, J. Mater. Chem. 7 (2019) 21730–21739.
[21] Q. Wang, C.C. Chueh, T. Zhao, M. Eslamian, W. Choy, A.K. Jen, Chemsuschem 10 (2017) 3794–3803.
[22] Y. Zhang, S. Zhang, S. Wu, C. Chen, H. Zhu, Z. Xiong, W. Chen, R. Chen, S. Fang, W. Chen, Adv. Mater. Interfaces 5 (2018) 1800645.
[23] T. Wang, D. Ding, X. Wang, R. Zeng, H. Liu, W. Shen, ACS Omega 3 (2018) 18434–18443.
[24] T. Wang, D. Ding, H. Zheng, X. Wang, J. Wang, H. Liu, W. Shen, Sol. RRL 3 (2019) 1900045.
[25] H. Fan, H. Wang, J. Guo, N. Zhao, J. Xu, J. Colloid Interface Sci. 414 (2014) 46–49.
[26] T. Liu, J. Hao, B. Yang, B. Hu, Z. Cui, S. Li, AAPS PharmSciTech 19 (2018) 1582–1591.
[27] Y. Wang, W. Fu, J. Yan, J. Chen, W. Yang, H. Chen, J. Mater. Chem. 6 (2018) 13090–13095.
[28] J.C. Yu, S. Badgujar, E.D. Jung, V.K. Singh, D.W. Kim, J. Gierschner, E. Lee, Y. S. Kim, S. Cho, M.S. Kwon, M.H. Song, Adv. Mater. 31 (2019) 1805554.
[29] F. Zhang, J. Song, R. Hu, Y. Xiang, J. He, Y. Hao, J. Lian, B. Zhang, P. Zeng, J. Qu, Small 14 (2018) 1704007.
[30] N.D. Pham, V.T. Tiong, D. Yao, W. Martens, A. Guerrero, J. Bisquert, H. Wang, Nano Energy 41 (2017) 476–487.
[31] J. Yun, J. Jun, H. Yu, K. Lee, J. Ryu, J. Lee, J. Jang, J. Mater. Chem. 5 (2017) 21750–21756.
[32] S. Wang, Z. Ma, B. Liu, W. Wu, Y. Zhu, R. Ma, C. Wang, Sol. RRL 2 (2018) 1800034.
[33] F. Zhou, H. Liu, X.W. Wang, W.Z. Shen, Adv. Funct. Mater. 27 (2017) 1606156.
[34] X. Yin, P. Chen, M. Que, Y. Xing, W. Que, C. Niu, J. Shao, ACS Nano 10 (2016) 3630.
[35] J. He, E. Bi, W. Tang, Y. Wang, Z. Zhou, X. Yang, H. Chen, L. Han, Sol. RRL 2 (2018) 1800004.
[36] S. Bag, M.F. Durstock, ACS Appl. Mater. Interfaces 8 (2016) 5053–5057.

[37] L. Gao, S. Huang, L. Chen, X. Li, B. Ding, S. Huang, G. Yang, Sol. RRL 2 (2018) 1800088.
[38] X. Zhou, Y. Zhang, W. Kong, M. Hu, L. Zhang, C. Liu, X. Li, C. Pan, G. Yu, C. Cheng, B. Xu, J. Mater. Chem. 6 (2018) 3012–3021.
[39] Y. Wu, P. Wang, S. Wang, Z. Wang, B. Cai, X. Zheng, Y. Chen, N. Yuan, J. Ding, W. H. Zhang, ChemSusChem 11 (2018) 837–842.
[40] D. Yang, X. Zhang, K. Wang, C. Wu, R. Yang, Y. Hou, Y. Jiang, S. Liu, S. Priya, Nano Lett. 19 (2019) 3313–3320.
[41] S.S. Mali, H. Kim, H.H. Kim, E.S. Sang, K.H. Chang, Mater. Today 21 (2018) 483–500.
[42] Y. Chen, Z. Yang, S. Wang, X. Zheng, Y. Wu, N. Yuan, W.H. Zhang, S.F. Liu, Adv. Mater. 30 (2018) 1805660.
[43] K. Yao, F. Li, Q. He, X. Wang, Y. Jiang, H. Huang, A.K.Y. Jen, Nano Energy 40 (2017) 155–162.
[44] D. Yang, R. Yang, K. Wang, C. Wu, X. Zhu, J. Feng, X. Ren, G. Fang, S. Priya, S. F. Liu, Nat. Commun. 9 (2018) 3239.
[45] Y. Cai, Z. Zhang, Y. Zhou, H. Liu, Q. Qin, X. Lu, X. Gao, L. Shui, S. Wu, J. Liu, Electrochim. Acta 261 (2018) 445–453.
[46] L. Yang, M. Wu, F. Cai, P. Wang, R.S. Gurney, D. Liu, J. Xia, T. Wang, J. Mater. Chem. 6 (2018) 10379–10387.
[47] J. Chen, L. Zuo, Y. Zhang, X. Lian, W. Fu, J. Yan, J. Li, G. Wu, C.-Z. Li, H. Chen, Adv. Energy Mater. 8 (2018) 1800438.
[48] M.A. Mahmud, N.K. Elumalai, M.B. Upama, D. Wang, K.H. Chan, M. Wright, C. Xu, F. Haque, A. Uddin, Sol. Energy Mater. Sol. Cells 159 (2017) 251–264.
[49] W.J. Scheideler, N. Rolston, O. Zhao, J. Zhang, R.H. Dauskardt, Adv. Energy Mater. 9 (2019) 1803600.
[50] J. Zheng, L. Hu, J.S. Yun, M. Zhang, C.F.J. Lau, J. Bing, X. Deng, Q. Ma, Y. Cho, W. F. Fu, ACS Appl. Energy Mater. 1 (2018) 561–570.
[51] M. Li, X. Xu, Y. Xie, H.-W. Li, Y. Ma, Y. Cheng, S.-W. Tsang, J. Mater. Chem. 7 (2019) 9578–9586.
[52] R. Blossey, Nat. Mater. 2 (2003) 301–306.
[53] P.Q.M. Nguyen, L.-P. Yeo, B.-K. Lok, Y.-C. Lam, ACS Appl. Mater. Interfaces 6 (2014) 4011–4016.
[54] X. Chen, P. Qian, T. Zhang, Z. Xu, C. Fang, X. Xu, W. Chen, P. Wu, Y. Shen, S. Li, Chem. Commun. 54 (2018) 3936–3939.